Freezing and correlations in fluids with competing interactions

2006 J. Phys.: Condens. Matter 18 S2305

(http://iopscience.iop.org/0953-8984/18/36/S06)

INSTITUTE OF PHYSICS PUBLISHING JOURNAL OF PHYSICS: CONDENSED MATTER

J. Phys.: Condens. Matter **18** (2006) S2305–S2320 doi:10.1088/0953-8984/18/36/S06

Freezing and correlations in fluids with competing interactions

D Pini[1], **A Parola**[2] **and L Reatto**[1]

[1] Dipartimento di Fisica, Università di Milano, Via Celoria 16, 20133 Milano, Italy
[2] Dipartimento di Scienze Fisiche, Università dell'Insubria, Via Valleggio 11, 22100 Como, Italy

E-mail: davide.pini@mi.infm.it

Received 9 February 2006, in final form 5 March 2006
Published 24 August 2006
Online at stacks.iop.org/JPhysCM/18/S2305

Abstract

We consider fluids in which the attractive interaction at distances slightly larger than the particle size is dominated at larger distances by a repulsive contribution. A previous investigation of the effects of the competition between attraction and repulsion on the liquid–vapour transition and on the correlations is extended to the study of the stability of liquid–vapour phase separation with respect to freezing. We find that this long-range repulsive part of the interaction expands the region in which the fluid–solid transition preempts the liquid–vapour one, so the critical point becomes metastable at longer attraction ranges than those required for purely attractive potentials. Moreover, the large density fluctuations that occur near the liquid–vapour critical point are greatly enhanced by the competition between attractive and repulsive forces, and encompass a much wider region than in the attractive case. The decay of correlations for states in which the compressibility is large is governed by two characteristic lengths, and the usual Ornstein–Zernike picture breaks down except for the very neighbourhood of the critical point, where one length reduces to the commonly adopted correlation length, while the other one saturates at a finite value.

1. Introduction

The attraction between the particles of a fluid is generally the dominant contribution to the overall interaction at distances slightly larger than the particle size σ. When a longer-ranged repulsion is also present, the interaction turns from attractive to repulsive as the distance is increased beyond σ, resulting in the so-called *mermaid potential* (attractive head and repulsive tail). It is well known that, even though the integrated intensity of the interaction remains negative, the phase diagram of the fluid can be deeply affected by the presence of a repulsion at long distance. In fact, when the repulsion strength is large enough, the liquid–vapour transition that would take place in the purely attractive case is inhibited, because the creation of a bulk dense phase becomes energetically unfavoured. As the temperature is lowered, the

fluid particles instead arrange themselves into a nonhomogeneous state [1, 2] with a modulated density, typically a cluster- or stripe-shaped configuration. In off-lattice systems like that considered here, this phenomenon has been observed experimentally in a number of cases [3], including colloidal films of metallic particles coated by a surfactant [4], and it has been investigated by numerical simulations in two-dimensional model fluids [5, 6]. The competing interaction scenario has recently gained much attention because of its relevance in colloidal systems, in which the repulsion may be due to electrostatic interactions or nonideal depletant agents. Cluster formation induced by competing interactions is frequently found in this context, and it has been detected for instance in colloid–polymer mixtures [7, 8], star–linear polymer mixtures [9], and protein solutions [8]; it can play an important role even in the dynamical arrest transition [10].

On the other hand, the competition between the attractive and the repulsive part of the potential strongly influences the behaviour of the system even in the regime in which the liquid–vapour transition has not yet been replaced by the occurrence of a nonhomogeneous state. In a previous study [11], we focused on this situation by considering a model fluid with a two-body potential given by the superposition of an attractive Yukawa tail with inverse-range parameter z_1 and a longer-ranged, repulsive one with inverse-range parameter z_2, and a strength not large enough to cause microphase separation. In that work we used liquid-state theory to study the thermodynamics and the correlations of the fluid when the amplitude of the repulsion is increased so as to approach the stability limit of the liquid–vapour transition. We found that there are three main effects that occur close to this limit: (i) the size of the region in the temperature–density plane in which the compressibility is large is remarkably bigger than the near-critical region of a fluid with purely attractive interaction; (ii) the top of the liquid–vapour coexistence curve becomes very flat, so the transition is nearly first order; (iii) the two-body correlations in the region of large compressibility have a faster decay at long distance than in the purely attractive case, but on the other hand they are strongly enhanced at short and intermediate distance, ranging from near contact up to several times and even several tens of the particle size. This behaviour indicates that the density fluctuations responsible for the large values of the compressibility must be traced back to the appearance of delocalized clusters of strongly correlated particles. These can be considered as the precursors of the nonhomogeneous phases that eventually set in for strong enough repulsion. The correlation function can then be approximately split into an intra-cluster and an inter-cluster contribution, each governed by a characteristic length.

In the aforementioned investigation we were almost exclusively concerned with the liquid–vapour transition. Little attention was paid to the freezing transition, whose location was just estimated by means of the Hansen–Verlet criterion [12] for a specific choice of the inverse-range parameters $z_1 = 1$, $z_2 = 0.5$ in units of σ^{-1}. In that case the freezing line was confined in the high-density region, well beyond the liquid–vapour critical point, and, unlike the liquid–vapour transition, it did not appear to be qualitatively affected by the competition between attraction and repulsion.

In view of the rekindled interest in these systems, a more thorough investigation is worth being pursued. Therefore, in the present paper we have extended our previous study by considering the freezing and melting transitions for a wide choice of the range of the interatomic interaction. Our aim in doing this is twofold. On the one hand, we would like to determine when the liquid–vapour transition is stable with respect to freezing, so that the modification in the shape of the liquid–vapour coexistence curve due to the competing interactions can actually be observed. On the other hand, we are also interested in finding out whether the freezing transition itself can be affected by this competition. To clarify these points, we have employed the self-consistent Ornstein–Zernike approximation (SCOZA) for the fluid, which we already

used in our previous work [11], and supplemented it by standard thermodynamic perturbation theory for the solid phase. Compared to the semi-empirical freezing criteria, which are based on indicators of the transition purely in the fluid phase, either structural (Hansen–Verlet [12]) or entropic (Giaquinta–Giunta [13]), this approach has the advantage of yielding both the freezing and the melting line, and above all it is expected to remain reliable even for interactions with narrow attractive parts.

According to our results, in most cases the stability of the liquid–vapour transition with respect to freezing is determined by the inverse range z_1 of the attractive part of the potential: when z_1 is small enough, or conversely large enough, the qualitative shape of the phase diagram is basically the same as we would expect for a purely attractive interaction with the same value of z_1, showing respectively a stable or a metastable liquid–vapour transition. However, there exists an intermediate interval of z_1, roughly between $z_1 = 3$ and 6 in units of σ^{-1}, in which the repulsive contribution to the interaction strongly influences the location of the liquid–vapour transition with respect to the fluid–solid one: while in the purely attractive case this range of z_1 yields stable liquid–vapour phase separation, we find that the latter is preempted by freezing for suitable values of the amplitude A and inverse range z_2 of the repulsion. Although this regime does not cover a very wide parameter range, it is nevertheless interesting to consider it, since when it occurs, the fluid–solid transition is affected by the peculiar behaviour of the thermodynamics and correlations already discussed in [11] and summarized in points (i)–(iii) above. Specifically, one observes large values of the compressibility and very strong correlations along a wide portion of the liquidus line. The enhancement of the compressibility is considerably stronger than that found in fluids with short-ranged, purely attractive interactions when the metastable liquid–vapour critical point lies in the neighbourhood of the liquidus line.

A second point we want to address in the present paper is a more thorough investigation of the behaviour of the correlation function and of the structure factor $S(q)$. In fluids with purely attractive tail potentials, the long-range behaviour of the correlations in the region in which the compressibility is large is well described in the Ornstein–Zernike (OZ) picture by an exponential decay with a certain characteristic length, namely the usual correlation length. On the other hand, when competing interactions are present, the OZ form is of limited use, save for the very neighbourhood of the critical region. In general, a double-exponential tail with two characteristic lengths is necessary in order to model the decay of the correlations, and $1/S(q)$ has to be represented by terms up to q^4.

The paper is organized as follows. In section 2 we give a brief sketch of the SCOZA and we review the perturbation theory for the solid phase that we used together with the SCOZA to obtain the fluid–solid equilibrium lines. In section 3 we discuss our results for the stability of the liquid–vapour transition with respect to freezing and how the latter is affected by the competing interactions. In section 4 we focus on the behaviour of the correlations. In section 5 we draw our conclusions.

2. Theory

Our model interaction is the hard-core plus two-Yukawa (HCTY) tail potential that we already considered in [11]:

$$v(r) = \begin{cases} \infty & r \leqslant \sigma, \\ \epsilon\sigma \left\{ -\dfrac{1}{r} \exp[-z_1(r/\sigma - 1)] + \dfrac{A}{r} \exp[-z_2(r/\sigma - 1)] \right\} & r > \sigma. \end{cases} \tag{1}$$

Here σ is the hard-sphere diameter, ϵ is the interaction strength, z_1, z_2 are the inverse range parameters of the attractive and repulsive contribution respectively, and $A > 0$ is the relative

amplitude of the repulsive contribution. In the following we will always assume that $z_1 > z_2$, so that $v(r)$ is attractive at distances slightly larger than σ, but becomes repulsive at long distance. The SCOZA for the HCTY potential has already been described in [14], so a detailed derivation of the theory will be omitted here. We just recall that this approach can be regarded as a generalization of the mean spherical approximation (MSA) [15]. In both the MSA and the SCOZA, the spatial dependence of the direct correlation function $c(r)$ for $r > \sigma$ is assumed to be the same as that of the tail potential $v(r)$. However, in the SCOZA the amplitude K of $c(r)$ is regarded as an *a priori* unknown function of the thermodynamic state, which must be determined by imposing the consistency between the compressibility and the internal energy route to thermodynamics. This constraint is embodied in the condition

$$\frac{\partial}{\partial\beta}\left(\frac{1}{\chi_{\rm red}}\right) = \rho\frac{\partial^2 u}{\partial\rho^2}, \tag{2}$$

where ρ is the number density, $\beta = 1/(k_{\rm B}T)$ is the inverse temperature, $\chi_{\rm red}$ is the reduced compressibility determined as the structure factor $S(k)$ at $k = 0$, and u is the excess internal energy per unit volume determined as the spatial integral of the potential $v(r)$ weighted by the radial distribution function $g(r)$. When the expressions for $\chi_{\rm red}$ and u in terms of $c(r)$ and $g(r)$ are substituted into equation (2), one obtains a partial differential equation (PDE) for the amplitude $K(\rho,\beta)$, which is solved numerically. When the tail potential is given by a one- or two-Yukawa form, or even by a linear superposition of Yukawas, one can take advantage of a wealth of analytical results [16] for the Ornstein–Zernike equation relating $c(r)$ to $h(r) \equiv g(r) - 1$, and this considerably simplifies the solution procedure.

As stated in the section 1, the main purpose of the present investigation of the mermaid potential (1) is the determination not only of the liquid–vapour phase boundary as already done in [11], but also of the fluid–solid one, for which we need the free energies of both the fluid and solid phases. While the free energies of the liquid and the vapour have been obtained by the SCOZA, for the free energy of the solid we have resorted to standard thermodynamic perturbation theory. This can be regarded as the application to a solid reference system of the perturbative expansion in powers of the inverse temperature β originally developed for a fluid by Barker and Henderson [17]. The Helmholtz free energy per particle $F_{\rm s}/N$ of a solid of N particles interacting via a hard-sphere plus tail potential then reads

$$\frac{\beta F_{\rm s}}{N} = \frac{\beta F_{\rm s}^{\rm HS}}{N} + 2\pi\beta\rho\int_0^\infty {\rm d}r r^2 g_{\rm s}^{\rm HS}(r)v(r) + \frac{\beta F_2}{N} + \mathcal{O}(\beta^3), \tag{3}$$

where $F_{\rm s}^{\rm HS}$ and $g_{\rm s}^{\rm HS}$ are the Helmholtz free energy and the radial distribution function of the hard-sphere solid averaged over the solid angle, and $\beta F_2/N$ denotes the second-order term in β. Solid-state perturbation theory has been adopted for studying fluid–solid equilibrium [18] and how it is affected by the range of the interaction [19–21]. This approach lacks the flexibility of density-functional theory, since it assumes that the perturbed system has the same crystal structure as the hard-sphere solid. Nevertheless, when this is the case, use of the truncated expansion (3) for the solid phase has proved to be quite reliable, actually considerably more so than in the fluid region [21]. In [22], equation (3) was used together with the SCOZA to study the phase diagram of a hard-core fluid with a narrow attractive Yukawa tail, and the results were found to be very satisfactory. Following the treatment given there, equation (3) has been truncated at the second-order term in β, which has then been estimated by an approximation suggested by Barker and Henderson [17], namely

$$\frac{\beta F_2}{N} \simeq -\pi\beta^2\rho\chi_{\rm s}^{\rm HS}\int_0^\infty {\rm d}r r^2 g_{\rm s}^{\rm HS}(r)v^2(r), \tag{4}$$

where $\chi_{\rm s}^{\rm HS}$ is the compressibility of the hard-sphere solid divided by the ideal-gas value. The Helmholtz free energy of the hard-sphere crystal needed in equation (3) has been determined

by integrating with respect to density the equation of state (EOS) given by Hall [23], which expresses the compressibility factor $Z = \beta P/\rho$ of the hard-sphere solid as an expansion in powers of the relative deviation of the density from its value at close packing $\rho_{\rm cp} = \sqrt{2}\sigma^{-3}$. As in [22], the integration constant is given by the value of $F_{\rm s}^{\rm HS}$ at a density $\rho = 0.736\rho_{\rm cp}$, for which we have used the result for the excess free energy with respect to the ideal gas $\beta F_{\rm ex}^{\rm HS}/N = 5.918\,89$, also reported in [22], determined via numerical simulation by Frenkel. The radial distribution function of the hard-sphere solid has been represented by the parameterization of Kincaid and Weis [24] with 60 neighbour shells [25]. This corresponds to a maximum interparticle separation slightly larger than eight times the nearest-neighbour distance d, which in turn is at most about $d \simeq 1.125\sigma$ in the density range for the solid phase that we investigated. In practice, we cut off the integrals appearing in equations (3), (4) at $r_0 = 8\sigma$, and then we added a long-range correction by setting $g_{\rm s}^{\rm HS}(r) \equiv 1$ for $r > r_0$. Such a correction is important only for the longest-ranged potentials among those considered here. Fluid–solid equilibria were determined by equating the pressure and the chemical potential of the fluid phase determined by the SCOZA with those of the solid phase given by equations (3), (4).

It should be noted that for this procedure to be a viable one, it is essential that the reference hard-sphere system is described at the same level of accuracy in both phases. Specifically, use of the accurate Hall EOS for the hard-sphere solid requires that the Carnahan–Starling (CS) equation [15], or one of comparable accuracy, is used for the fluid. When the CS EOS is used, the hard-sphere freezing and melting densities are found to be $\rho_{\rm f} = 0.942\sigma^{-3}$ and $\rho_{\rm m} = 1.041\sigma^{-3}$ respectively, in very good agreement with the simulation values $\rho_{\rm f} = 0.945\sigma^{-3}$, $\rho_{\rm m} = 1.041\sigma^{-3}$. However, describing the hard-sphere fluid by the Percus–Yevick (PY) EOS [15] would fail to give a fluid–solid transition for this system, and consequently for the potential (1) in the high-temperature limit. This consideration is relevant in the present context, since our formulation of the SCOZA represents the direct correlation function $c(r)$ for $r > \sigma$ as the superposition of two Yukawa functions, both of which are needed to represent the tail of the HCTY potential (1). As a consequence, there should be no off-core contribution to $c(r)$ due to the purely hard-core part of $v(r)$, and this would indeed yield a PY description of the hard-sphere fluid. The conceptually most straightforward way to include the CS EOS into the SCOZA is to resort to the Waisman parameterization [26] for the hard-sphere contribution to $c(r)$, so that the full $c(r)$ for $r > \sigma$ takes a three-Yukawa form. Such a treatment has been developed by other authors, and generalized to a linear combination of n Yukawa tails [27] as well as to a linear combination of Yukawa and exponential tails [28], albeit so far the applications do not include the mermaid potential considered here. For the sake of computational simplicity, we have instead resorted to an ad hoc modification of the two-Yukawa SCOZA, which consists in assuming that the hard-sphere contribution to $c(r)$ outside the repulsive core has a Yukawa form with the same inverse-length parameter z_1 as the shorter-ranged part of $v(r)$, and a density-dependent amplitude $H(\rho)$ which is set so as to give the CS EOS. As a consequence, in the full $c(r)$ the amplitude of the shorter-ranged Yukawa is given by $H(\rho) + K(\rho, \beta)$ rather than by $K(\rho, \beta)$ alone, where $H(\rho)$ is a known function, and $K(\rho, \beta)$ is determined by the thermodynamic consistency condition (2) as specified above. This method has been illustrated in greater detail in [16], where it was used to study an HCTY interaction with amplitudes and ranges fitted to a Lennard-Jones potential. The resulting liquid–vapour coexistence curve was found to be both accurate and very close to that subsequently obtained [29] for the same interaction by the three-Yukawa formulation of the SCOZA: the relative difference in the critical points does not exceed 0.33%. Perhaps more surprisingly, the radial distribution function also appeared to be little affected by our ad hoc assumption on the hard-sphere contribution to $c(r)$ [14]. To get an estimate of how much the location of

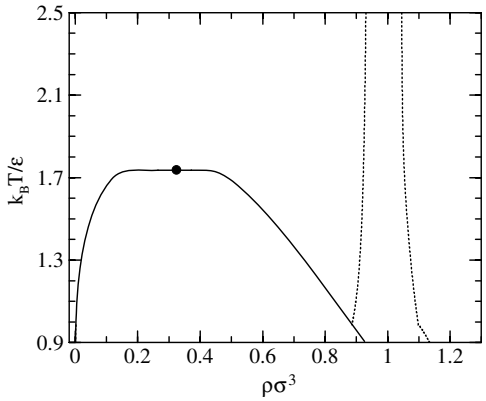

Figure 1. Phase diagram of the hard-core two-Yukawa fluid with competing interactions (see equation (1)) in the density–temperature plane according to the SCOZA supplemented by perturbation theory for the solid phase (see text). The potential parameters are $z_1 = 1$, $z_2 = 0.5$, $A = 0.0976$. Solid line: liquid–vapour coexistence. Dotted line: fluid–solid coexistence. Full circle: liquid–vapour critical point.

the fluid–solid phase boundary is affected by this prescription, we set $A = 0$ in equation (1), so as to get the same hard-core Yukawa (HCY) interaction that was studied in [22]. For this interaction, the Waisman description of the hard-sphere reference fluid is achieved within our two-Yukawa SCOZA, and in fact this is the approach that has been used in that work. We then employed the simplified treatment of the hard-sphere reference fluid adopted here to determine the value of the inverse range z_1 at which the liquid–vapour transition becomes metastable with respect to the fluid–solid one, and compared it with that obtained in [22]. That calculation gave $z_1 = 6.05$, in close agreement with the Gibbs ensemble Monte Carlo (GEMC) result $z_1 = 6$ by Hagen and Frenkel [20], while here we get $z_1 = 5.7$. We regard this 5% discrepancy with respect to the more complete treatment as a tolerable one, especially in view of the fact that the considerations developed in this work are mainly qualitative.

3. Phase diagram

In the following we will adopt reduced quantities $T^* = k_BT/\epsilon$, $\beta^* = \beta\epsilon$, $\rho^* = \rho\sigma^3$. The SCOZA PDE that we used for the fluid phase has been solved numerically on a grid of (β^*, ρ^*) values. The reduced density interval extended from $\rho^* = 0$ up to an high-density boundary ρ_0^*. This was set at $\rho_0^* = 1$ for potentials with relatively long-ranged attractive parts, for example for inverse-range parameter $z_1 = 1.8$. For short-ranged interactions, the liquid–vapour coexistence curve rapidly extends to high densities as the temperature is lowered, and the high-density boundary was therefore moved to higher values, up to $\rho_0^* = 1.4$ for the case $z_1 = 7$. The integration was stopped at a value of β^* large enough to obtain a significant portion of the liquid–vapour coexistence curve. The pressure and the chemical potential of the solid phase needed to determine the fluid–solid equilibrium lines were obtained by numerical differentiation of the solid free energy given by equations (3), (4).

In figure 1 we show the phase diagram corresponding to the inverse-range parameters $z_1 = 1$, $z_2 = 0.5$ that were already considered in [11]. The amplitude of the repulsive tail was set at the value $A = 0.0976$, at the stability limit of the bulk liquid–vapour transition. For slightly larger values of A, our numerical algorithm fails to converge before the liquid–vapour critical point is reached, and we take this as an indication that, as the temperature is lowered,

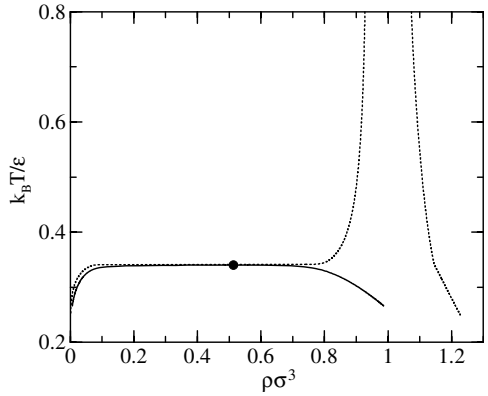

Figure 2. Same as figure 1 with $z_1 = 3$, $z_2 = 1.8$, $A = 0.29$.

the system would undergo a transition into a nonhomogeneous phase. This cannot be described by a liquid-state theory such as the SCOZA, which assumes the fluid to be homogeneous. We observe that the boundary value of A is little affected by the ad hoc procedure described in section 2 to ensure that the SCOZA recovers the CS hard-sphere EOS in the limit $\beta \to 0$. The relative difference with respect to the value obtained using PY hard-sphere thermodynamics as in [11] does not exceed 0.3%. For this choice of parameters, the system shows stable vapour, liquid, and solid phases with a triple point. This is in agreement with what we found in [11] by means of the Hansen–Verlet criterion for freezing [12]. The phase diagram illustrated in figure 1 is representative of the situation that we found at small values of z_1. Specifically, we chose $z_1 = 1$ and $z_1 = 2$ and considered several values of z_2, namely $z_2 = 0.25$, 0.5, 0.75, 0.9 for $z_1 = 1$, and $z_2 = 1.5$, 1.8, 1.9 for $z_1 = 2$. In all of these cases, we found that freezing never preempts the liquid–vapour transition in the whole range of repulsion strength A at which the latter occurs. We recall that on increasing A within this range, the critical temperature decreases. As we observed in [11], there is a trivial contribution to this effect which is to be expected already at the mean-field level, just because the integrated intensity of the (overall attractive) potential decreases in absolute value as A is increased. However, close to the boundary value of A, where the repulsion affects more deeply the behaviour of the fluid, the drop in the critical temperature becomes much sharper than that given by mean-field theory. For a given value of z_1, the decrease in the critical temperature with respect to that of the purely attractive case gets larger as the inverse range of the repulsion z_2 gets closer to z_1. Nevertheless, this does not imply that by taking the two ranges very similar, the liquid–vapour coexistence curve will be pushed below the freezing curve, thereby having freezing preempt liquid–vapour phase separation. In fact, the limit $z_1 = z_2$ amounts to a trivial rescaling of the interaction strength with respect to the purely attractive case $A = 0$, which is not going to affect the shape of the phase diagram, provided of course the sign of the potential remains negative.

We now consider larger values of z_1. Figure 2 shows the phase diagram for $z_1 = 3$, $z_2 = 1.8$, $A = 0.29$. The situation has changed with respect to that illustrated in figure 1, since here the liquid–vapour coexistence curve is tangent to the freezing line, and disappears into the fluid–solid coexistence region for larger values of A, until the stability limit of bulk phase separation is reached. For the case shown in figure 2, this happens for $A = 0.295$, which gives a metastable liquid–vapour critical temperature differing from that of the flat part of the liquidus line by about 10%. A similar behaviour is found, for instance, for $z_1 = 4$, $z_2 = 1.8$, and $0.15 \leqslant A \leqslant 0.17$, the largest relative difference in temperature between the metastable

critical point and the plateau of the liquidus line being now around 25%. We observe that in this regime one finds a metastable liquid–vapour coexistence curve for an inverse range z_1 of the attractive tail that is significantly smaller than the threshold value for metastability with purely attractive interactions. The latter, as we said in section 2, amounts to $z_1 = 5.7$ in the approximation used here. It may then be worthwhile looking more closely at the origin of the metastability in the present case. A possible explanation is that, as A is increased, the repulsive part of the potential leads to a decrease in the effective range of the attractive contribution, which in turn makes the liquid–vapour critical point become metastable, just as in fluids with short-ranged attractive interactions. However, this is not always the case: for instance, the profile of the potential for the parameter choice $z_1 = 3$, $z_2 = 1.8$, $A = 0.29$ to which figure 2 refers, is indeed narrower than a single attractive tail with $z_1 = 3$, but nevertheless it is quite wider than the tail corresponding to the threshold range $z_1 = 5.7$. A quantitative comparison can be made by means of the prescription for determining the effective attraction range proposed by Noro and Frenkel [30] in order to give a unified description of the phase behaviour of fluids with different attractive potentials. For a given interaction, this temperature-dependent range is defined as the width of the square-well potential which yields the same reduced second virial coefficient $B_2(T)/B_2^{\mathrm{HS}}$ at the same reduced temperature $k_{\mathrm{B}}T/v(\sigma)$, where the reduced quantities are obtained by rescaling the temperature T and the second virial coefficient $B_2(T)$ by the depth of the attractive well $v(\sigma)$ and by the hard-sphere second virial coefficient $B_2^{\mathrm{HS}} = 2\pi\sigma^3/3$ respectively. If we adopt this mapping for the case just mentioned, we find that at the critical temperature the effective range of the interaction with $z_1 = 3$, $z_2 = 1.8$, $A = 0.29$ is 40% larger than that of the purely attractive interaction with $z_1 = 5.7$, $A = 0$, despite the fact that both of them give a liquid–vapour coexistence curve tangent to the freezing line. Therefore, trying to predict the phase diagram of a fluid with competing interactions on the basis of the effective range alone may turn out to be tricky, even before bulk phase separation disappears. In fact, Noro and Frenkel [30] observed that, unlike interactions whose off-core part is purely attractive, potentials that include repulsive barriers do not lend themselves to a universal description in terms of their effective range. However, we note that, in the region in which the liquidus line broadens, the rescaled temperature $k_{\mathrm{B}}T/v(\sigma)$ is little affected by the repulsion. This agrees with what was found by Louis [31, 32] for fluids with deep attractive wells. For these 'energetic fluids', he determined an approximate crystallization criterion [32], according to which the freezing density becomes about 50% of that of the hard-sphere fluid when one has $\beta v(\sigma) \simeq 2.4 \pm 0.3$, where $\beta v(\sigma)$ is the reciprocal of the rescaled temperature. Specifically, for the above-mentioned cases $z_1 = 5.7$, $A = 0$; $z_1 = 4$, $z_2 = 1.8$, $A = 0.15$; $z_1 = 3$, $z_2 = 1.8$, $A = 0.29$; we find that the liquidus line broadens to half the hard-sphere freezing density for $\beta v(\sigma) = 2.15$, $\beta v(\sigma) = 2.17$, and $\beta v(\sigma) = 2.08$ respectively, in fair agreement with Louis' criterion. Such a result strongly suggests that even in the regime to which figure 2 refers, in which the liquid–vapour transition would be stable in the absence of repulsion, it is still the effective strength $\beta v(\sigma)$ of the attraction at contact that causes the metastability of liquid–vapour phase separation. This occurs when the inverse critical temperature β_{c} is large enough for $\beta_{\mathrm{c}} v(\sigma)$ to exceed the threshold value at which the liquidus line broadens. Therefore, the change in the phase diagram from stable to metastable liquid–vapour transition is triggered essentially by the same mechanism as in the case of narrow attractive potentials. The only difference is that here we have a sort of additional degree of freedom with respect to a purely attractive interaction, inasmuch as the increase of the rescaled inverse critical temperature $\beta_{\mathrm{c}} v(\sigma)$ beyond the threshold for metastability can be induced not only by decreasing the attraction range, but also by increasing the strength of the repulsion for suitable choices of the inverse-range parameters z_1, z_2 so as to approach the boundary of bulk phase separation, where the critical temperature drops quickly. In the latter case, the liquid–

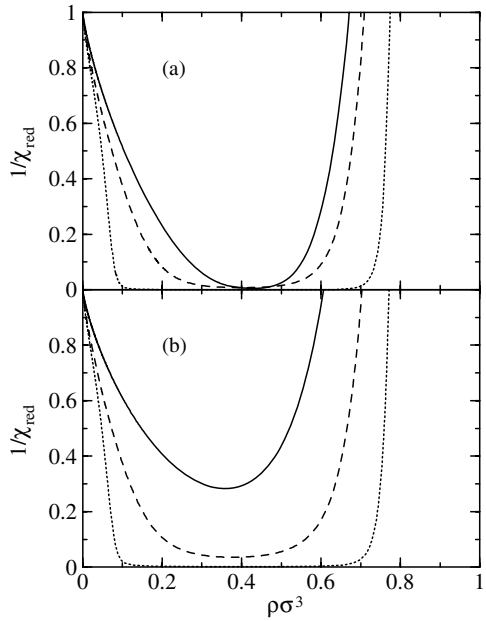

Figure 3. Inverse reduced compressibility $1/\chi_{red}$ along the liquidus line for different interaction profiles. The interaction parameters have been chosen so that in panel (a) the liquid–vapour coexistence curve is tangent to the liquidus line, while in panel (b) it is metastable, the flat part of the liquidus line corresponding to a temperature about 8% above that of the liquid–vapour critical point. Panel (a): solid line, $z_1 = 5.7$, $A = 0$; dashed line, $z_1 = 4$, $z_2 = 1.8$, $A = 0.15$; dotted line, $z1 = 3$, $z_2 = 1.8$, $A = 0.29$. Panel (b): solid line, $z_1 = 7$, $A = 0$; dashed line, $z_1 = 4$, $z_2 = 1.8$, $A = 0.16$; dotted line, $z_1 = 3$, $z_2 = 1.8$, $A = 0.294$.

vapour transition can become metastable at potential ranges that are significantly larger than those required for purely attractive interactions.

Moreover, the proximity to the stability limit for the existence of the homogeneous fluid phases implies that the effects on the thermodynamics which are characteristic of that regime, summarized in section 1, show up along and in the neighbourhood of the liquidus line. For instance, in figure 2 this line shares with the liquid–vapour coexistence curve the very flat portion that develops in the latter shortly before the repulsion amplitude A reaches its boundary value. As a consequence, on lowering the temperature the liquidus line broadens even more abruptly than in fluids with narrow attractive interactions. The effect on the density fluctuations is shown in figure 3, that compares the reciprocal of the reduced compressibility $1/\chi_{red}$ along the liquidus line for a purely attractive tail interaction and for the cases $z_1 = 3$, $z_2 = 1.8$ and $z_1 = 4$, $z_2 = 1.8$. In panel (a), the inverse range of the attractive interaction and the amplitudes of the repulsive tail have been chosen so that the liquidus line is tangent to the liquid–vapour coexistence curve. While the compressibility obviously always increases as the critical point is approached, the size of the region in which it remains large is greatly enhanced by the competition between attraction and repulsion. This region increases not only in density but also in temperature, as shown in panel (b), in which the interaction parameters have been adjusted so that the flat part of the liquidus line lies above the metastable liquid–vapour critical temperature by about 8%. As the liquid–vapour coexistence curve sinks below the liquidus line, the $1/\chi_{red}$ versus ρ curve corresponding to the purely attractive potential is pulled upward much more quickly than those of the fluids with competing interactions. In

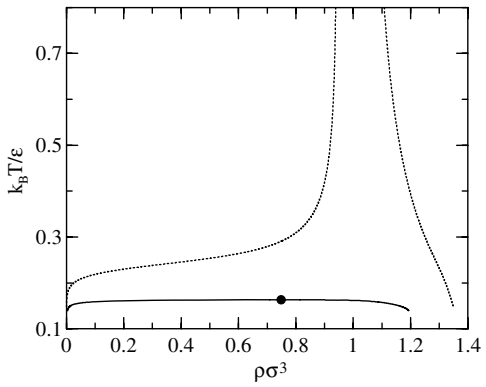

Figure 4. Same as figure 1 with $z_1 = 7$, $z_2 = 4$, $A = 0.4$.

summary, in the intermediate interval of z_1 just considered, the strong density fluctuations induced by the competing interactions markedly affect the behaviour of the fluid in the region of the liquidus line, even though the metastability of the liquid–vapour transition is always driven by the strength of the attraction near contact.

Finally, we turn to the case where the inverse range z_1 of the attractive part of the interaction is large enough to give a metastable liquid–vapour transition even in the absence of repulsion. In this regime, the liquid–vapour transition remains *a fortiori* metastable when the repulsion is turned on. As A is increased, the temperature of the metastable critical temperature decreases more quickly than that of the plateau of the liquidus line, so the liquid–vapour coexistence curve never gets out of the fluid–solid coexistence region. Therefore, the effects on the thermodynamics and correlations that come along because of the competing interactions always involve the domain of the metastable fluid. An example of the phase diagram corresponding to this situation is shown in figure 4 for $z_1 = 7$, $z_2 = 4$, $A = 0.4$. The metastable liquid–vapour coexistence curve exhibits the very flat shape that one finds close to the boundary value of A ($A = 0.42$ in the present case), beyond which no bulk fluid–fluid phase separation is predicted by the theory.

A quite relevant issue is the role played by the freezing transition when the strength of the repulsion becomes large enough to give rise to the formation of inhomogeneous phases. Specifically, one might ask whether in this regime of short-ranged attraction the freezing transition will preempt the occurrence of microphases just as it preempts the liquid–vapour transition at lower values of A. A fully satisfactory answer cannot be given within the present investigation, since, as we noted above, our theoretical approach cannot deal with nonuniform phases. However, we can try and increase A enough to get into the region of interaction parameters in which the fluid is expected to become inhomogeneous at low enough temperature. We then find that the temperature at which our algorithm does not yield solutions rapidly increases with A. For the inverse-range choice $z_1 = 7$, $z_2 = 4$ to which figure 4 refers, it is sufficient to raise the repulsion strength slightly above $A = 0.5$ to find that, at the lowest isotherm that we can attain, the freezing line has not yet developed a plateau. This suggests that for high enough A, the formation of microphases will not be preempted by freezing, even when the attractive part of the interaction is short-ranged. The fact that the temperature of the transition from the homogeneous to the density-modulated phase should increase as the repulsion strength is increased is not surprising, and is in agreement with the results obtained in lattice systems with competing interactions [33].

4. Correlations

As already observed in [11], competing interactions deeply affect the correlations, even in the region in which the system is still in the fluid phase. In the OZ picture, the behaviour of the correlations in the region in which the compressibility is large is obtained by assuming a parabolic shape for the reciprocal of the structure factor $S(q)$ at small wavevector q, $1/S(q) \sim a + bq^2$ with $a = 1/\chi_{\rm red}$. This gives

$$h(r) \sim \frac{1}{4\pi\rho b}\left(1 - \frac{1}{\chi_{\rm red}}\right)\frac{1}{r}\exp(-r/\xi) \tag{5}$$

for the asymptotic decay of the two-body correlation function $h(r)$, where $\xi = \sqrt{b/a}$ is the usual correlation length. As is well known, the assumption that $1/S(q)$ is analytic in q breaks down at the critical point, but even there it is still a reasonable approximation, because in three-dimensional fluids the deviations from analyticity are small. However, when the strength A of the repulsive part of the potential is large enough for the system to be close to the stability limit of bulk liquid–vapour phase separation, the coefficient b can be very small. The link between b and the interaction is particularly straightforward within the random-phase approximation (RPA), in which this coefficient is proportional to the second moment of the tail potential. In the RPA scenario, the limit of bulk phase separation is indeed reached at that value of A for which b vanishes. For larger values of A, b becomes negative, so $S(q)$ changes its convexity at $q = 0$. The peak of $S(q)$ then moves away from the origin, and eventually develops into a singularity at nonzero q at low temperature. In more sophisticated approaches, such as the SCOZA used here, the explicit form of b cannot be worked out so easily, since this involves the state-dependent amplitude $K(\rho, \beta)$, which is *a priori* unknown, and is also expected to be a functional of the interaction itself. Nevertheless, it is still true that increasing the repulsion strength A leads in general to a decrease and eventually to a negative value of b. For large enough A the SCOZA structure factor displays, in addition to the usual particle–particle peak at $q \simeq 2\pi/\sigma$, the characteristic peak at smaller q related to cluster–cluster correlations [8–10]. However, as the temperature is lowered, the theory eventually fails to converge since, as observed in section 3, the SCOZA cannot describe the formation of inhomogeneous microphases.

Even in the regime in which the liquid–vapour transition still exists but the competition between attraction and repulsion is strong, the quadratic approximation for $1/S(q)$ at small q is expected to become a poor one, since higher-order terms become important. This is shown in figure 5. In panel (a) we have plotted the SCOZA results for $1/S(q)$ as a function of q^2 for two fluids with and without competing interactions, namely for $A = 0.29$, $z_1 = 3$, $z_2 = 1.8$ and for $A = 0$, $z_1 = 3$. In the latter case, we have $\rho^* = \rho_{\rm c}^* = 0.359$, $t = (T - T_{\rm c})/T_{\rm c} = 6.45 \times 10^{-4}$. For the competing interaction case, the density has again been set to the critical value $\rho_{\rm c}^* = 0.515$ and the reduced temperature is $t = 2.81 \times 10^{-2}$. The reduced compressibilities are similar for the two states, $\chi_{\rm red} = 1.61 \times 10^3$ and $\chi_{\rm red} = 1.67 \times 10^3$ respectively. While for purely attractive interactions $1/S(q)$ is a nearly linear function of q^2 in the interval of q reported in the figure, there are marked deviations from linearity when competing interactions are present. These deviations persist even at densities away from the critical one, as shown by the result for $\rho^* = 0.1$, $t = 3.50 \times 10^{-3}$, $\chi_{\rm red} = 71.3$, also plotted in the figure, which lies very close to the liquidus line. One is then led also to take into account the q^4-term in the expansion of $1/S(q)$ by setting

$$1/S(q) \sim a + bq^2 + cq^4. \tag{6}$$

To which extent this can be considered a good approximation is shown in panel (b) of figure 5, which shows the derivative of $1/S(q)$ with respect to q^2 as a function of q^2. In this representation, equation (6) gives a straight line with an intercept b and a slope $2c$, the

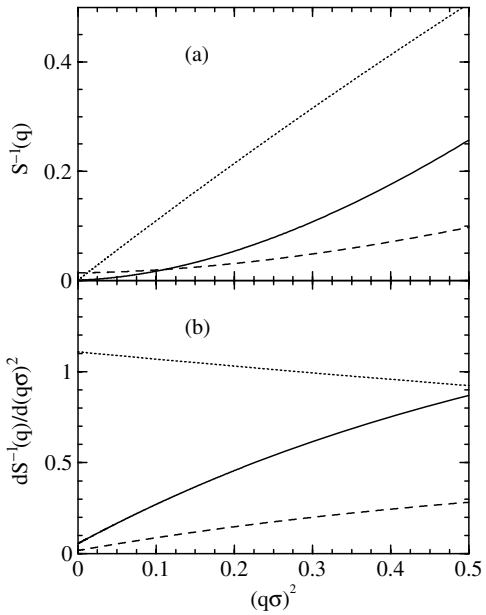

Figure 5. Panel (a): reciprocal of the structure factor $1/S(q)$ as a function of q^2 with and without competing interactions for the potential parameters and the thermodynamic states described in the text. Dotted line: $A = 0$, $z_1 = 3$, $\rho^* = \rho_c^* = 0.359$, $t = (T - T_c)/T_c = 6.45 \times 10^{-4}$. Solid line: $A = 0.29$, $z_1 = 3$, $z_2 = 1.8$, $\rho^* = \rho_c^* = 0.515$, $t = 2.81 \times 10^{-2}$. Dashed line: $A = 0.29$, $z_1 = 3$, $z_2 = 1.8$, $\rho^* = 0.1$, $t = 3.5 \times 10^{-3}$. Note the deviations from linearity when competing interactions are present. Panel (b): derivative of $1/S(q)$ with respect to q^2 as a function of q^2. Equation (6) gives a straight line on this plot.

standard OZ form corresponding to a horizontal line. It appears that in the fluid with competing interactions the q^4-term plays a much more important role than in the purely attractive case. Even for the low-density state $\rho^* = 0.1$, $t = 3.50 \times 10^{-3}$ for which the absolute value of the deviation from the OZ form is similar to that of the attractive case, the relative weight of the quartic term is nevertheless much bigger because of the much smaller value of b.

The long-range behaviour of the correlation function corresponding to equation (6) is obtained by a straightforward contour integration, and has the form [11]

$$h(r) = \frac{1}{4\pi\rho\sqrt{\Delta}}\left(1 - \frac{1}{\chi_{\mathrm{red}}}\right)\frac{1}{r}\left[\exp(-r/\lambda) - \exp(-r/\mu)\right], \tag{7}$$

where $\Delta = b^2 - 4ac$, and the lengths λ, μ are given by

$$\lambda = \left(\frac{2c}{b - \sqrt{\Delta}}\right)^{\frac{1}{2}}, \tag{8}$$

$$\mu = \left(\frac{2c}{b + \sqrt{\Delta}}\right)^{\frac{1}{2}}. \tag{9}$$

In figure 6 we have plotted the radial distribution function $g(r) = 1 + h(r)$ for the same interactions and thermodynamic states considered in figure 5. Unlike in the purely attractive case, the two-exponential form is indeed necessary to describe the long-range decay of the correlations. The usual OZ form (5) is recovered only asymptotically close to the critical point, where λ diverges and reduces to the usual correlation length ξ, while μ saturates at a finite

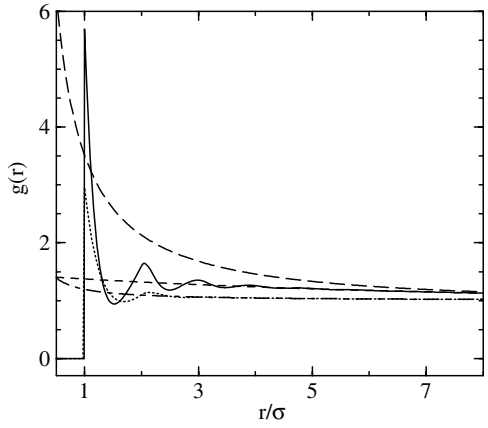

Figure 6. Radial distribution function $g(r)$ at the critical density for the potential parameters and thermodynamic states considered in figure 5. Solid line: $A = 0.29$, $z_1 = 3$, $z_2 = 1.8$, $\rho^* = 0.515$, $t = 2.81 \times 10^{-2}$, $\chi_{\rm red} = 1.67 \times 10^3$. Long-dashed line: long-range tail of $g(r)$ as predicted by the OZ equation (5). Dashed line: long-range tail of $g(r)$ as predicted by the double-exponential equation (7). Dotted line: $A = 0$, $z_1 = 3$, $\rho^* = 0.359$, $t = 6.45 \times 10^{-4}$, $\chi_{\rm red} = 1.61 \times 10^3$. Dot–dashed line: long-range tail of $g(r)$ as predicted by the OZ equation (5).

value. This does not apply to the situation shown in the figure, for which we find $\lambda = 7.80$, $\mu = 5.65$ in units of the hard-sphere diameter σ. Besides being comparable, these lengths are much smaller than the correlation length $\xi = 42.3\sigma$ of the purely attractive case. Since the compressibility is similar for the two states considered here, the slower decay of $h(r)$ in the attractive fluid must be compensated by larger values of $h(r)$ at small and intermediate r in the fluid with competing interactions. This is the reason for the enhancement of the correlations induced by the competition in the range of r shown in the figure.

Equations (7)–(9) are also formally valid for $b < 2\sqrt{ac}$, but they do not appear physically transparent in this case, since λ and μ become complex conjugate quantities, and $h(r)$ presents damped oscillations at large r. In this regime, equations (7)–(9) are more conveniently rewritten as follows:

$$h(r) = \frac{1}{2\pi\rho\sqrt{|\Delta|}}\left(1 - \frac{1}{\chi_{\rm red}}\right)\frac{1}{r}\sin(r/\delta)\exp(-r/\zeta), \tag{10}$$

$$\delta = 2\left(\frac{c}{2\sqrt{ac} - b}\right)^{\frac{1}{2}}, \tag{11}$$

$$\zeta = 2\left(\frac{c}{2\sqrt{ac} + b}\right)^{\frac{1}{2}}. \tag{12}$$

It is interesting to observe that the asymptotic decay of $g(r)$ can be oscillatory even for states in which the compressibility is large. The occurrence of monotonic and oscillatory regimes for the decay of the correlations, governed respectively by the characteristic lengths (8), (9) and (11), (12), was obtained before by other authors [34] in a general study of $O(n)$ spin models with competing ferro- and antiferromagnetic interactions. In fact the effect discussed above stems from rather general features of the interaction and appear close to the limit of bulk fluid–fluid phase separation irrespective of the specific choice of the competing-interaction potential, provided of course the amplitude A of the repulsion is tuned so that one is indeed close to that limit. They can be relevant also for the correlations along the liquidus line, if the interaction parameters are such that this line enters the large-fluctuation region as it broadens to

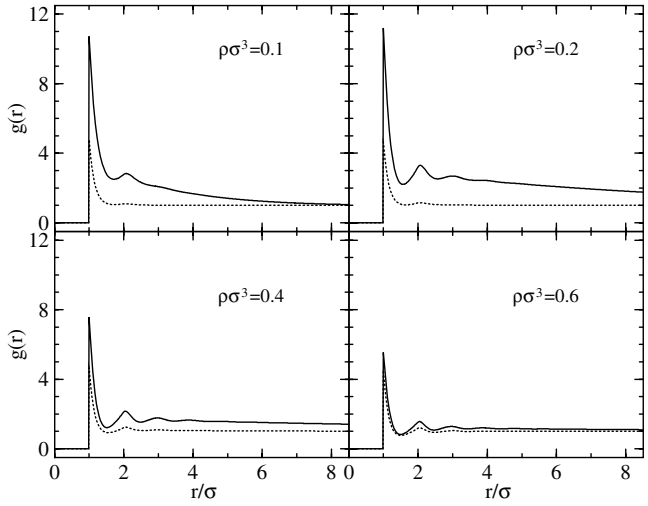

Figure 7. Radial distribution function $g(r)$ along the liquidus line for $z_1 = 5.7$, $A = 0$ (dotted line) and $z_1 = 3$, $z_2 = 1.8$, $A = 0.29$ (solid line). Each panel corresponds to a different density.

low density. One then expects the behaviour of the correlations to be different from that found along the liquidus line of purely attractive fluids. The two situations are compared in figure 7, in which $g(r)$ is shown at several densities along the liquidus line for $z_1 = 5.7$, $A = 0$ and $z_1 = 3$, $z_2 = 1.8$, $A = 0.29$. For both of these sets of parameters, as observed above, the liquidus line is tangent to the liquid–vapour coexistence curve. For systems with narrow attractions, it has been observed by Louis [32] that, in the region in which the liquidus line broadens, the two-body radial distribution function $g(r)$ is well approximated by the zeroth-order term of its expansion in powers of the density, $g(r) \simeq \exp[-\beta v(r)]$, in a remarkably wide density interval. As a consequence, varying the density within this interval has little effect on $g(r)$. While the $g(r)$ corresponding to the purely attractive tail is indeed relatively unaffected by density, that of the fluid with competing interactions deviates almost immediately from its low-density limit, and is strongly enhanced both near contact and at larger values of r as soon as large density fluctuations develop. We recall that in the SCOZA the direct correlation function is linear in the off-core part of the interaction, as in the MSA. As a consequence, the $g(r)$ obtained by the theory does not reproduce the exact zeroth-order term of the density expansion, and shows some quantitative inaccuracies, especially near contact, where it underestimates the correct values. Nevertheless, we expect the qualitative behaviour shown in figure 7 to be genuine.

5. Conclusions

We have used the SCOZA to study the correlations in fluids with competing interactions consisting of the sum of an attractive Yukawa tail and a longer-ranged, repulsive one. Our results show that the competition between attraction and repulsion causes the appearance of strong density fluctuations in a relatively large region of the temperature–density plane. In this regime, the usual OZ picture, according to which the correlations in the critical region are described in terms of a single correlation length, is replaced by a scenario in which two characteristic lengths are necessary to describe the long-range behaviour of the correlations. We have also considered the freezing transition and the stability of liquid–vapour phase separation with respect to freezing by supplementing the SCOZA with thermodynamic perturbation theory

for the solid. We find that in most cases the character of the liquid–vapour transition is determined by the range of the attractive contribution: potentials with long- or short-range attractive parts give a liquid–vapour critical point which lies respectively outside and inside the fluid–solid coexistence region. However, at intermediate attraction ranges one can have freezing preempt the liquid–vapour transition by suitably tuning the repulsive contribution, and the region of large fluctuations encompasses the liquidus line. It would be interesting to find out if this effect can be relevant for nucleation, especially of the solid phase in the fluid [35]. We finally remark that we focused on a two-Yukawa potential because it leads to a semi-analytic formulation of the SCOZA. However, the effects discussed here appear to hinge on quite general features of the competition between attraction and repulsion as the stability limit of bulk fluid–fluid phase separation is approached. Therefore, they are expected to occur also in different systems with competing interactions [34].

Acknowledgment

We acknowledge support from the Marie Curie program of the European Union, contract number MRTN-CT2003-504712.

References

[1] Brazovskiĭ S A 1975 *Zh. Eksp. Teor. Fiz.* **68** 175
Brazovskiĭ S A 1975 *Sov. Phys.—JETP* **41** 85 (Engl. Transl.)
[2] Andelman D, Broçhard F and Joanny J F 1987 *J. Chem. Phys.* **86** 3673
[3] Seul M and Andelman D 1995 *Science* **267** 476
[4] Gelbart W M, Sear R P, Heath J R and Chaney S 1999 *Faraday Discuss.* **112** 299
[5] Sear R P, Chung S W, Markovich G, Gelbart W M and Heath J R 1999 *Phys. Rev.* E **59** R6255
[6] Imperio A and Reatto L 2004 *J. Phys.: Condens. Matter* **16** S3769
[7] Campbell A I, Anderson V J, van Duijneveldt J S and Bartlett P 2005 *Phys. Rev. Lett.* **94** 208301
[8] Stradner A, Sedgwick H, Cardinaux F, Poon W C K, Egelhaaf S U and Schurtenberger P 2004 *Nature* **432** 492
[9] Stiakakis E, Petekidis G, Vlassopoulos D, Likos C N, Iatrou H, Hadjichristidis N and Roovers J 2005 *Europhys. Lett.* **72** 664
[10] Sciortino F, Mossa S, Zaccarelli E and Tartaglia P 2004 *Phys. Rev. Lett.* **93** 055701
[11] Pini D, Jialin G, Parola A and Reatto L 2000 *Chem. Phys. Lett.* **327** 209
[12] Hansen J P and Verlet L 1969 *Phys. Rev.* **184** 151
[13] Giaquinta P V and Giunta G 1992 *Physica* A **187** 145
[14] Pini D, Stell G and Wilding N B 2001 *J. Chem. Phys.* **115** 2702
[15] See, for instance Hansen J P and McDonald I R 1986 *Theory of Simple Liquids* (London: Academic)
[16] Høye J S, Stell G and Waisman E 1976 *Mol. Phys.* **32** 209
Høye J S and Stell G 1984 *Mol. Phys.* **52** 1057
Høye J S and Stell G 1984 *Mol. Phys.* **52** 1071
[17] Barker J A and Henderson D 1967 *J. Chem. Phys.* **47** 2856
[18] Weis J J 1974 *Mol. Phys.* **28** 187
Hecht C E and Lind J 1976 *J. Chem. Phys.* **64** 641
Kincaid J M, Stell G and Goldmark E 1976 *J. Chem. Phys.* **65** 2172
[19] Gast A P, Russell W B and Hall C K 1983 *J. Colloid Interface Sci.* **96** 1977
Gast A P, Russell W B and Hall C K 1986 *J. Colloid Interface Sci.* **109** 161
[20] Hagen M H J and Frenkel D 1994 *J. Chem. Phys.* **101** 4093
[21] Dijkstra M, Brader J M and Evans R 1999 *J. Phys.: Condens. Matter* **11** 10079
[22] Foffi G, McCullagh G D, Lawlor A, Zaccarelli E, Dawson K A, Sciortino F, Tartaglia P, Pini D and Stell G 2002 *Phys. Rev.* E **65** 031407
[23] Hall K R 1972 *J. Chem. Phys.* **57** 2252
[24] Kincaid J M and Weis J J 1977 *Mol. Phys.* **34** 931
[25] Hirschfelder J O, Curtis C F and Bird R B 1954 *The Molecular Theory of Gases and Liquids* (New York: Wiley)
[26] Waisman E 1973 *Mol. Phys.* **25** 45

[27] Kahl G, Schöll-Paschinger E and Stell G 2002 *J. Phys.: Condens. Matter* **14** 9153
Schöll-Paschinger E and Kahl G 2003 *Europhys. Lett.* **63** 538
Costa D, Pellicane G, Caccamo C, Schöll-Paschinger E and Kahl G 2003 *Phys. Rev.* E **68** 21104
[28] Schöll-Paschinger E 2004 *J. Chem. Phys.* **120** 11698
[29] Schöll-Paschinger E 2002 *Doctoral Thesis* University of Wien
[30] Noro M G and Frenkel D 2000 *J. Chem. Phys.* **113** 2941
[31] Louis A A, Finken R and Hansen J P 2000 *Phys. Rev.* E **61** R1028
[32] Louis A A 2001 *Phil. Trans. R. Soc.* A **359** 939
[33] Selke W 1992 *Phase Transition and Critical Phenomena* vol 15, ed C Domb and J L Lebowitz (New York: Academic)
[34] Nussinov Z, Rudnick J, Kivelson S A and Chayes L 1999 *Phys. Rev. Lett.* **83** 472
[35] ten Wolde P R and Frenkel D 1997 *Science* **277** 1975